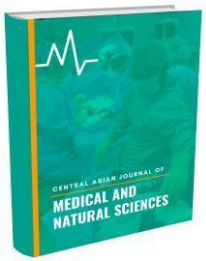

CENTRAL ASIAN JOURNAL OF MEDICAL AND NATURAL SCIENCES
https://cajmns.centralasianstudies.org/index.php/CAJMNS
Volume: 06 Issue: 03 | July 2025 ISSN: 2660-4159

Article

Structural and Crystalline Properties Analysis of Nanomaterials Using Electron Diffraction Techniques

Zainab Alwan Adhib[1]

1. Ministry of Education - General Directorate of Education, Thi Qar

Abstract: In this research, we present a fast and easy method for analyzing electron diffraction patterns of randomly selected areas (SAED) without the need to rotate or tilt the sample. The goal is to determine the crystalline phase and unit cell by combining the outcomes with software for X-ray diffraction (XRD). After determining the pattern's center, the two-dimensional (2D-SAED) pattern can be easily transformed into a one-dimensional (1D-profile) file if the Transmission Electron Microscope (TEM) is calibrated correctly and the camera length is accurately adjusted. After precisely detecting the peaks or matching the file, this file is then input into XRD analysis tools, allowing phase identification and unit cell determination. The method was tested and validated using two nanomaterials: TiO_2 with a flaky structure and TiO_2 nanotubes deposited with silver nanoparticles. The method also demonstrated success in crystalline analysis of a single gold nanoparticle crystal, indicating its potential use in analyzing small-sized nanocrystals, although it may require using two or more tilted SAED patterns. If dependable integrated diffraction intensity can be derived, this method can be extended for quantitative phase analysis, structural determination, and enhancing Rietveld refinement models for nanomaterials.

Keywords: Electron Diffraction, SAED, Nanomaterials, X-Ray Diffraction (XRD), Crystal Phase Identification, Unit Cell Determination, TEM, Rietveld Refinement, Tio_2, Silver Nanoparticles, Gold Nanocrystals

Citation: Adhib, Z. A. Structural and Crystalline Properties Analysis of Nanomaterials Using Electron Diffraction Techniques. Central Asian Journal of Medical and Natural Science 2025, 6(3), 1000-1009.

Received: 22th Mar 2025
Revised: 25th Mar 2025
Accepted: 8th Apr 2025
Published: 4th May 2025

1. Introduction

Because of the special qualities of nanomaterials, which range in size from 1 to 100 nm, as well as their potential uses in a wide range of sectors, nanoscience and technology have advanced significantly since the 1990s. These materials have demonstrated efficacy in a number of fields, such as chemical catalysis [1], environmental pollution control [2], photonics and plasmonics [3], [4], [5], [6], [7], and information storage [8]. Finding the crystal phase and the unit cell are crucial problems in the creation and research of nanomaterials since crystal structure, shape, and particle size are all closely related to these functional properties.

The most popular method for determining the crystal structure of bulk materials is X-ray diffraction (XRD), which has developed over the course of more than a century to become one of the most sophisticated analytical techniques. It is backed by a thorough diffraction theory as well as freely and commercially available analysis software. However, the use of XRD techniques for analyzing nanomaterials is still limited for several reasons, including:

1. Low yield of prepared nanomaterials, which may not be sufficient for X-ray experiments.
2. Long exposure times (up to several hours or days) are required for X-ray diffraction patterns to be obtained in high quality.
3. Data processing becomes more difficult when there are overlapping Kα2 reflections in the high angular range because of the broadening of diffraction peaks caused by poor crystallinity of nanomaterials and high density of defects and crystal boundaries.

However, because electrons interact strongly with the nucleus and with other electrons in the scattering centers, electron diffraction has a scattering power 10^4 to 10^5 times that of X-rays. Because of this, even during brief exposure times (just a few seconds), electron diffraction patterns can be produced from extremely small quantities of sample. Furthermore, accelerated electrons have a wavelength that is far shorter than that of neutrons or X-rays. For instance, electrons accelerated at 200 keV have a wavelength of around 0.0250793 Å, which is significantly shorter than that of a typical X-ray tool (1.5406 Å for a Cu anode). The diffraction patterns surrounding the transmitted beam are concentrated as a result of the extremely narrow Bragg angles.

To get a symmetric diffraction pattern in traditional selected area electron diffraction (SAEDP) patterns, the sample needs to be tilted and rotated to a low-index axis (ZAP). Rebuilding the 3D reciprocal space allows for the extraction of the crystal lattice parameters (a, b, c, α, β, γ) of the unknown phase [9]. However, nanosamples ranging in size from one nanometer to several hundred nanometers may not be amenable to tilting or rotation. The sample may change during electron irradiation, even if a ZAP pattern is properly obtained. This makes indexing and phase analysis more challenging.

Additionally, it is uncommon to employ direct SAED for crystallographic investigation of nanomaterials; instead, high-resolution transmission electron microscopy (HRTEM), convergent beam diffraction (CBED), and microbeam diffraction are employed. This is because conventional TEM allows the selection of analysis areas of at least 500 nm with similar error limits.

Furthermore, even though the idea of electron crystallography has been presented and used to quantitative crystal phase analysis, crystallographic study of nanoparticles remains a challenging and time-consuming process. In this work, we suggest a novel, quick, and simple technique that uses a single SAED electron diffraction pattern to conduct unit cell determination and crystal phase identification directly without rotating or tilting the sample.

2. Materials and Methods

The dynamic effect has a major impact on the diffraction intensity for electron diffraction since the electron cross-section is much bigger than that of X-rays. However, because of the high density of surfaces and flaws, the intensity of diffraction peaks in nanoparticles is typically unpredictable. As a result, diffraction intensity-based quantitative analysis, including Rietveld purification, quantitative phase analysis, and structure determination, is likewise unreliable. Fortunately, the interatomic spacing (d-spacing) of diffraction peaks is more important for phase and unit cell identification, which can be carried out once these spacings have been carefully determined.

Similar to X-ray analysis, phase identification and unit cell determination of a selected area electron diffraction (SAED) pattern require the acquisition of the maximum number of diffraction spots and the most accurate inter-spacing of each diffraction spot. Thus, examples of solutions used in transmission electron microscopy (TEM) experiments are as follows:

A- Sample preparation: The sample must be thin enough for the electron beam to pass through, so nanomaterials with large particles (e.g., several hundred nanometers) must be reduced to smaller particles using ultrasound.

B- Changing the sample specification: The sample used in TEM research needs to contain an infinite number of nanoparticles with totally random orientations in order to produce a sufficient number of diffraction spots and a consistent diffraction intensity. As a result, a self-supporting grid can accommodate many tiny particles without worrying about their overlapping.

C- Pattern analysis: To fit the curves and offer accurate inter-diffraction peak spacing, the majority of X-ray diffraction (XRD) analysis algorithms employ the Pseudo-Voigt or Pearson VII function.

D- Alignment of the electron microscope: The camera length needs to be precisely calibrated and the electron microscope needs to be properly set before beginning an SAED experiment. The following is a summary of the general procedure for conducting experiments and analyzing data:

To do an SAED experiment, choose the sample of your choice and, without tilting or rotating it, capture random SAED patterns. The generated patterns will have a sufficient number of diffraction spots and dependable diffraction intensity if the chosen area has a high concentration of randomly oriented particles.

Setting up the electron microscope: The resolution of the SAED pattern is affected by focusing, the sample's eucentric height, the objective lens's standard voltage, and the condenser and intermediate lenses' aberration correction.

E- Digital data conversion: If the patterns were captured on film, they should be scanned and converted to digital format. Then, they should be calibrated using the DigitalMicrograph software to match the length of the camera or the drawing scale.

F- Data curve generation: The DigitalMicrograph software's profile tools can be used directly if the sample is sufficient. Difftools, RDF, or the PASAD package—all freely accessible online—should be used to extract the average circular curve if the sample has a certain texture.

G- Finding the SAED pattern's center: The SAED pattern's center should be precisely identified because it has a significant impact on peak locations. Any inaccuracy causes values on the 1/nm axis to shift, which complicates search and matching or results in an incorrect grid constant. Inaccurate center determination also leads to the expansion of the diffraction peaks and their accuracy, or even the appearance of multiple peaks after the rotational averaging process.

Data Formatting and Analysis

1) File Format: Most XRD analysis applications cannot directly use the generated file because it is in 1/nm vs. signal intensity format. As a result, it needs to be changed to the signal intensity format for Bragg angle (2θ)
2) Data Conversion: The relationship found between 2θ (in degrees) and 1/d (1/nm) is determined using Bragg's diffraction law. The diffraction source's wavelength is changed to 0.1 angstrom in order to provide a more precise investigation.
3) Crystallization Analysis: The data is instantly entered into the XRD analysis program after being converted to x-y format. This allows for precise peak locations to be found by curve fitting or peak searching.
4) Phase Matching: Using search and matching algorithms like MDI Jade, DIFFRAC + Eva, or Search-Match, the phase is ascertained based on the energy dispersive spectroscopy experiment (EDX), precise peaks, and known chemical information.
5) Cell Unit Determination: The authorized mathematical method is used to determine the cell unit in the event that the phase is unknown.

$$\frac{1}{d^2} = \left[\frac{h^2}{a^2 \sin^2 \alpha} + \frac{2kl}{bc} (\cos\beta\cos\gamma - \cos\alpha) + \frac{k^2}{b^2 \sin^2 \beta} + \frac{2hl}{ac} (\cos\alpha\cos\gamma - \cos\beta) + \frac{l^2}{c^2 \sin^2 \gamma} + \frac{2hk}{ab} (\cos\alpha\cos\beta - \cos\gamma) \right]$$
$$(1 - \cos^2\alpha - \cos^2\beta - \cos^2\gamma + 2\cos\alpha\cos\beta\cos\gamma)$$

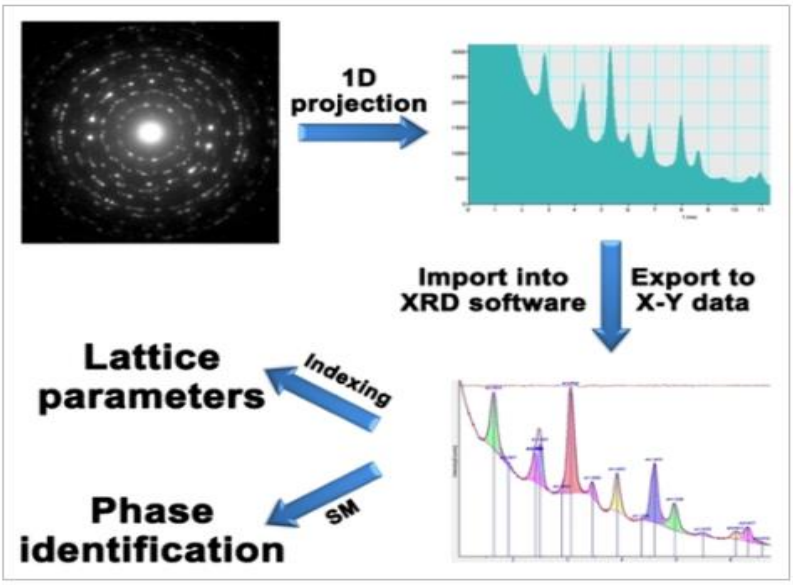

Figure 1. Schematic depiction of the experiment and overall analysis process.

Finding peaks in selected area electron diffraction (SAED) experiments or altering the file to determine the exact peak locations—to be used later for indexing or phase identification—creating a 1D profile of a 2D SAED pattern, exporting the data to an X-Y file, and then importing it into an X-ray diffraction (XRD) analysis program.

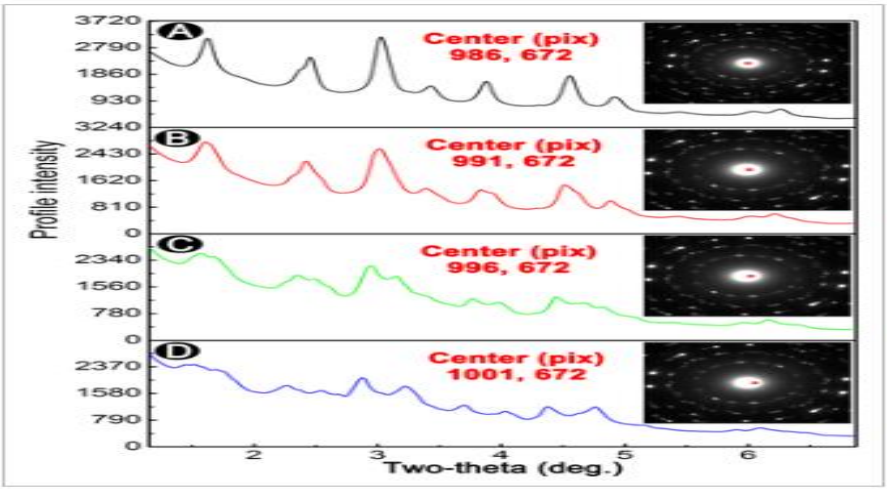

Figure 2. Pattern center's impact on diffraction peaks (A) Peaks with an exact center are distinct and well-defined; (B) peaks with a slight center displacement are broader. (C) and (D) Inaccurate center assignment causes numerous peaks to appear.

Where **(h k l)** are the triplet indices of the lattice planes and d is the crystal lattice's interplane distance. Lattice constants are represented by the six coefficients a, b, c, α, β, and γ. Using indexing software like Checkcell, Crysfire, Winplotr, MDI Jade, DIFFRAC plus Topas, etc., the corresponding unit cell dimensions are determined when all or some of the observed peaks have been allocated to the triplet (h k l). Lastly, the least squares method is used to adjust the calculated unit cell dimensions in order to produce more precise results.

3. Results and Discussion

Scanning electron microscopy (TEM) provides the benefit of real-time observation of the region of interest and analysis of its structure or chemical information through electron diffraction or energy dispersive X-ray (EDX) experiments, as opposed to relying on conventional X-ray diffraction (XRD) experiments to obtain average information. XRD reveals a multiphase mixture that could be orthorhombic, Ti2O3, or a 2D titanium phase [10]. On the other hand, nanomaterials like TiO2 can take on a variety of shapes, including nanorods, nanoparticles, nanotubes, and layered structures [11], [12], [13], [14]. We are now interested in figuring out which morphology matches which phase or structure, as this information can help us enhance our fabrication process.

The flaky fragments with particles of around 10 nm that usually form as clusters, as seen in the lower right corner of Figure 3, are now the focus of our TEM experiments, which simultaneously demonstrate the nanopillars and the flaky morphology. With an exposure length of 0.8 seconds, in the upper right corner, a random SAED pattern was recorded.. This pattern was random and irregular, indicating a textural effect and a small number of particles surrounding the transmitted beam. Next, using Difftools' rotating average, this SAED pattern was projected in a one-dimensional orientation around the center. The resulting X-Y data was then stored, and the peak pattern was presented similarly to the standard XRD experiments in Figure 3. An automatic peak search was performed once these data were imported into the MDI Jade software (the wavelength needs to be changed in "Preferences/Tool" under the "Edit" menu). The peak positions were shown by green lines. With a simple search and comparison, all of the detected peaks can be reliably assigned to the anatase phase (space group I41/a m d, shown by red bars).

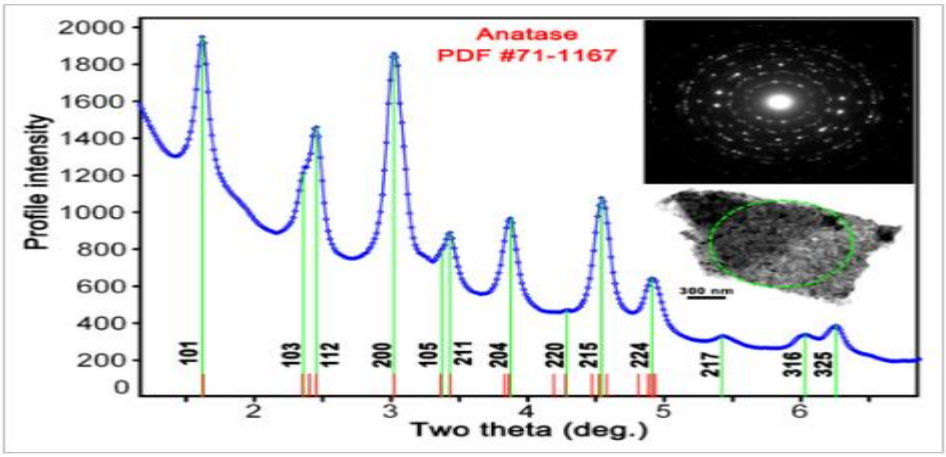

Figure 3. One-dimensional X-ray profile obtained from the region of interest (represented by a green dot circle) of the foil-like samples, based on the rotation average of the two-dimensional SAED pattern (upper right corner). Red bars represent the main phase (anthase phase: PDF #71–1167), and green lines show the positions of the experimental profile's peaks.

TiO2 nanotubes with silver nanoparticles on them provide yet another illustration of phase identification. Given that if the organic catalysts are not properly cleaned, organic contaminants usually accumulate on the tubes, we are unable to confirm that the dark or gray grains that were adsorbed on the nanotubes are actually silver nanoparticles, as displayed in the sample's TEM-BF (bright field image) image in Figure 4A. To determine the phases, a random SAED pattern (Fig. 4B) was extracted from the region of interest (represented by the green dot circle) and then displayed in a 1D file (Fig. 4C). According to the search and matching results, there are two phases in this sample: the silver phase (shown by blue lines) and the anatase phase (represented by red lines) [15], [16], [17], [18] [19]. The dark-field image (Figure 4D), which can be produced directly from the isolated peak at 2.05 Å, which corresponds to the {0 0 2} diffraction spots of the silver nanoparticles in Fig., clearly shows the form of the silver nanoparticles adsorbed on the TiO2 nanotubes. 4B (indicated by the red arrow).

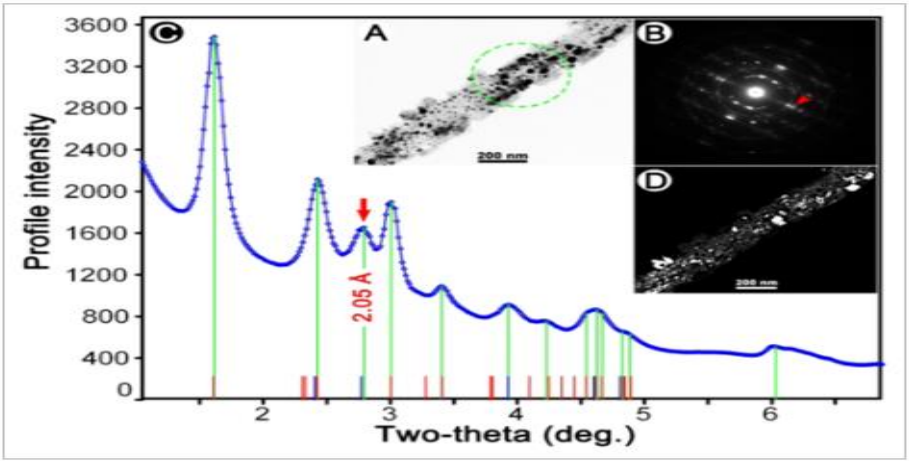

Figure 4. Shows the phase analysis of TiO2 nanotubes covered with silver nanoparticles.

1. This nanotube's bright-field picture;
2. B: A random SAED pattern from the green circle-denoted region of interest
3. This SAED pattern's 1D profile, which displays the silver phase as blue lines and the anatase phase as red lines.
4. A dark-field image made from the selected diffraction point in (B) and the peak at 2.05 Å in (C).

The file matching result for the TiO2 flake-like material is displayed in Figure 5, where MDI Jade was used to index the observed peaks indicated by green lines. Using a fast-indexing process, the cubic, hexagonal, tetragonal, and Swiss crystal systems were chosen for pattern indexing. The angular error window was set to 0.5, the angle limit to 9, the maximum cell to 20, and the fm-cutoff to 99. The first 10 indexing results in Table 1 show that the tetragonal crystal system (T), with the cell set at 3.795 Å 9.439 Å and the space group probability of I 41/a m d (No. 141), can index the TiO2 nanocrystals well. The first cell was then selected as the starting cell for the cell unit optimization. The findings indicate that the volume is 135.81 $Å^3$, the density is 3.907 g/cm^3, and the lattice parameters are 3.793)6) Å × 9.436(7) Å. These results are in good agreement with the previous phase identification result in Figure 3.

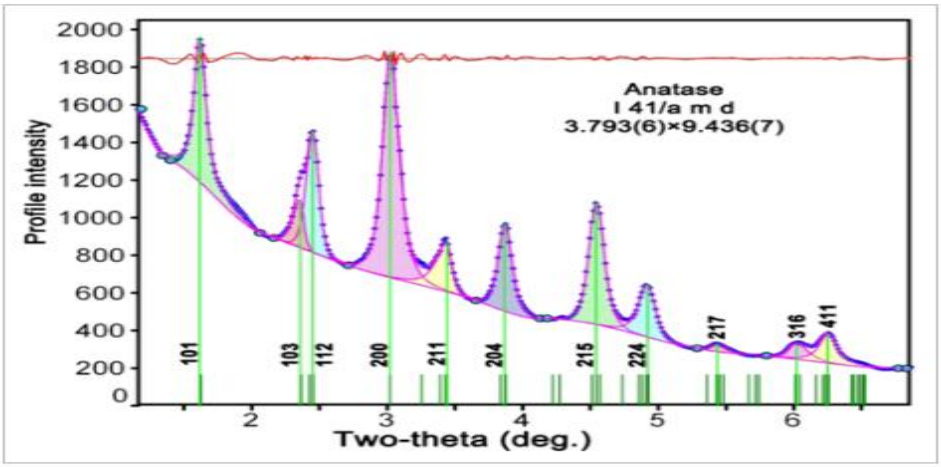

Figure 5. The TiO2 sample cell unit is indexing and optimization results are shown in Figure 5, where the optimized cell sites are represented as dark green bars and the peak positions utilized for indexing are indicated as green lines.

Table 1. The first 10 findings for the TiO2 flake pattern identification are similar samples, where "C" stands for the crystal system, "Fm" and "Fn" for the merit scale and its analog, and "P" and "R" for the number of unindexed peaks and reflections below the designated angle limit.

Fm	Fn	P	R	C	S. G.	a (Å)	b (Å)	c (Å)	α	β	Γ	Vol. (Å3)
79	40	0	29	T	I 41/a m d (141)	3.795	3.795	9.439	90	90	90	135.9
79	39	0	30	T	I 41 m d (109)	3.795	3.795	9.439	90	90	90	135.9
82	34	0	40	T	I 41 2 2 (98)	3.795	3.795	9.439	90	90	90	135.9
83	32	0	40	T	I 42 2 2 (97)	3.795	3.795	9.439	90	90	90	135.9
86	17	0	76	H	P 3 1 2 (149)	5.431	5.431	5.353	90	90	120	136.7
86	19	0	55	T	P 4/n n c (126)	3.796	3.796	9.367	90	90	90	135.0
86	25	0	58	T	P 4 n c (104)	3.795	3.795	9.437	90	90	90	135.9
86	19	0	73	T	P 41 2 2 (91)	3.793	3.793	9.445	90	90	90	135.9
87	24	0	60	H	P 63 2 2 (182)	5.431	5.431	9.445	90	90	120	136.7
87	24	0	59	H	P 62 2 2 (180)	5.431	5.431	9.445	90	90	120	136.7

Crystalline properties of single nanocrystal

Because of the small size of the scattering region and the single random orientation, when we wish to analyze a single nanocrystal (see the box in Figure 6E) with small grain size (several nanometers), we can acquire very few scattering spots for crystallographic characterization from a single random SAED pattern, such as Figs. 6A and 6B. Therefore, two or more arbitrarily tilted patterns must be blended in order to create a significant number of scattering areas in this scenario. The randomly slanted SAED patterns and 1D files of the nanocrystal are shown in Figures 6A–6D [20], [21], [22], [23] [24]. As shown by the resulting (basic combination) file of these arbitrarily tilted patterns in Fig. 6E, this nanocrystal matches the gold phase quite well, according to the search and matching process. The unit cell is a = b = c = 4.058(9) Å, the density is 19.56 g/cm3, and the volume is 66.87 Å3. The inter-spot distance between these two peaks is just around 0.0122 Å, and it should be mentioned that there is another peak at the front of the (3 3 3) lattice plane that is indicated by a red star. This might be the result of local lattice distortions brought on by the high pressures at this plane; for the majority of FCC nanocrystals, this phenomena typically manifests as stacking faults [25], [26].

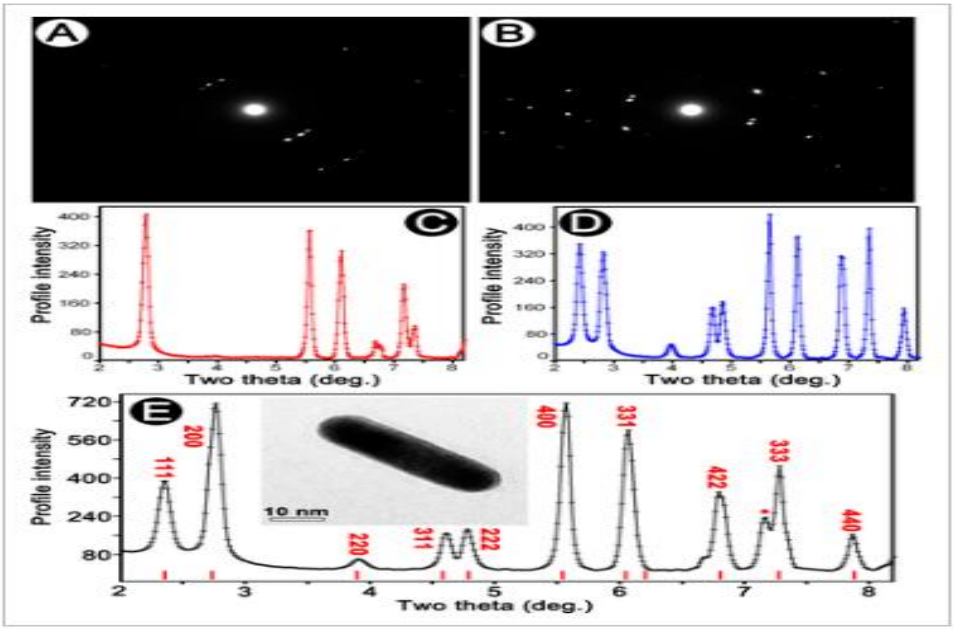

Figure 6. A single gold nanocrystal's crystallographic characterization is shown in Figure 6: (Two randomly chosen SAED tilting patterns are shown in A and B, their 1D profiles are shown in C and D, and the profile that emerges from C and D is shown in E. The back-image (BF) of the nanocrystal is shown in the frame, and the phase match is indicated by red markers.

4. Discussion

Some possible uses have been suggested based on prior experiences

Nanoscale phase identification: The distance between lattice planes is regarded as a structural fingerprint of a specific crystal with a given crystal system and lattice characteristics. Phase identification can be performed using non-random orientations at the nanoscale and a restricted number of scattering locations from a restricted number of nanocrystals. If EDX is available in the TEM in vivo, phase identification results will be more trustworthy.

Quantitative phase identification: According to the literature, spin-averaged projection can be used to extract dependable integrated scattering intensities from the scattering pattern, which can then be utilized in quantitative phase analysis for samples with less pronounced or preferred orientation [27].

Nonetheless, there are a few things to keep in mind in order to identify the phase:

1. Properly calibrated camera length is necessary to avoid a significant discrepancy between the observed peaks and the peaks that correspond to the PDF card;
2. Even though the PDF card has peaks, some scattered peaks could not be visible since there are not many samples or non-random crystals in that region.

It is crucial to remember that in order to obtain precise pattern recognition results:

1. The extracted file moves along the 2θ axis when the camera length is calibrated correctly, preventing zero deviation.
2. Carefully locating the center of the SAED pattern is essential to preserving the file's correctness during rotation average projection; otherwise, the entire width of the peaks (FWHM) may enlarge or several peaks may appear.
3. Astigmatism and C-Focus are also important components that affect the accuracy of SAED pattern.

5. Conclusion

In the current study, a quick and an easy method id devoted for employing the SAED pattern as a standard XRD analysis to identify the unit cell and phase of nanomaterials. Finding the pattern's center and creating a 1D file from a random 2D-SAED pattern are all that is required if the TEM is properly adjusted and the camera length is set. Once the file has been converted, it can be easily imported into XRD analysis software, allowing you to finally enjoy crystallographic analysis.

The dependable file will be obtained after spin-averaged projection (the dynamic effect should be considered) if you obtain a high-quality SAED pattern, such as a ring-like pattern from symmetric ZAP or completely randomly oriented samples. At the nanoscale, the integrated scattering intensity can then be utilized for Rietveld refinement and structural identification.. This technique can also be applied to electron beam scattering investigations or in vivo TEM studies to observe structural phase changes.

REFERENCES

[1] Crooks RM, Zhao MQ, Sun L, Chechik V, Yeung LK. 2001. Dendrimer-encapsulated metal nanoparticles: Synthesis, characterization, and applications to catalysis. Acc Chem Res 34: 181–190.

[2] Shrivastava VS. 2010. Metallic and organic nanomaterials and their use in pollution control: A review. Arch Appl Sci Res 2: 82–92.

[3] Kamat PV. 2002. Photophysical, photochemical and photocatalytic aspects of metal nanoparticles. J Phys Chem B 106: 7729–7744.

[4] Ozbay E, Guven K, Aydin K, Bayindir M. 2004. Physics and applications of photonic nanocrystals. Int J Nanotechnol 1: 379–398.

[5] Zhao YX, Pan HC, Lou YB, Qiu XF, Zhu JJ, Burda C. 2009. Plasmonic Cu2-xS nanocrystals: Optical and structural properties of copper-deficient copper (I) sulfides. J Am Chem Soc 131: 4253–4261.

[6] Jie G, Liu B, Pan H, Zhu JJ, Chen HY. 2007. CdS nanocrystal-based electrochemiluminescence biosensor for the detection of low-density lipoprotein by increasing sensitivity with gold nanoparticle amplification. Anal Chem 79: 5574–5581.

[7] Xu K, Huang J, Ye Z, Ying Y, Li Y. 2009. Recent development of nano-materials used in DNA biosensors. Sensors 9: 5534–5557.

[8] Gubin SP, Spichkin YI, Yurkov GY, Tishin AM. 2002. Nanomaterial for high-density magnetic data storage. Russ J Inorg Chem 47: 32–67.

[9] Zou XD, Hovmöller A, Hovmöller S. 2004. TRICE-A program for reconstructing 3D reciprocal space and determining unit-cell parameters. Ultramicroscopy 98: 187–193.

[10] Borghols WJH, Lutzenkirchen-Hecht D, Haake U, Chan W, Lafont U, Kelder EM, van Eck ERH, Kentgens APM, Mulder FM, Wagemaker M. 2010. Lithium Storage in Amorphous TiO2 Nanoparticles. J Electrochem Soc 157: A582–A588.

[11] Zhang M, Bando Y, Wada K. 2001. Sol-Gel Template Preparation of TiO2 nanotubes and nanorods. J Mater Sci Lett 20: 167–170.

[12] Liu B, Aydil ES. 2009. Growth of oriented single-crystalline rutile TiO2 nanorods on transparent conducting substrates for dye-sensitized solar cells. J Am Chem Soc 131: 3985–3990.

[13] Roy P, Kim D, Lee K, Spiecker E, Schmuki P. 2010. TiO2 nanotubes and their application in dye-sensitized solar cells. Nanoscale 2: 45–59.

[14] Gupta SM, Tripathi M. 2011. A review of TiO2 nanoparticles. Chin Sci Bull 56: 1639–1657.

[15] Kim G, Ahn, JP. 2006. Phase identification of nano-phase material using convergent beam electron diffraction (CBED) technique. Korean J Electron Microsc 1: 47–56; special issue.

[16] Kumar V. 2011. Automated grain mapping using wide angle convergent beam electron diffraction in transmission electron microscope for nanomaterials. Microsc Microanal 17: 859–865.

[17] Li XZ. 2012. QPCED2.0: A computer program for the processing and quantification of polycrystalline electron diffraction patterns. J Appl Crystallogr 45: 862–868.

[18] Mitchell DDRG. 2008. DiffTools: Electron diffraction software tools for DigitalMicrograph™. Microsc Res Tech 71: 588–593.

[19] Gammer C, Mangler C, Rentenberger C and Karnthaler HP. 2010. Quantitative local profile analysis of nanomaterials by electron diffraction. Scripta Mater 63: 312–315.

[20] Mitchell DRG, Petersen TC. 2011. RDFTools: A software tool for quantifying short-range ordering in amorphous materials. Microsc Res Tech 75: 153–163.

[21] Neogy S, Savalia RT, Tewari R, Srivastava D, Dey, GK. 2006. Transmission electron microscopy of nanomaterials. Indian J Pure Appl Phys 44: 119–124.

[22] Vineet K. 2011. Automated grain mapping using wide angle convergent beam electron diffraction in transmission electron microscope for nanomaterials. Microsc Microanal 17: 859–865.

[23] Weirich TE, Lábár JL, Zou XD. 2006. Electron crystallography: Novel approaches for structure determination of nanosized materials. Dordrecht: Springer.

[24] Yun YH, Eteshola E, Bhattacharya A, Dong Z, Shim JS, Conforti L, Kim D, Schulz MJ, Ahn CH, Watts N. 2009. Tiny medicine: Nanomaterial-based biosensors. Sensors 9: 9275–9299.

[25] Zehetbauer M, Valiev RZ. 2004. Nanomaterials by severe plastic deformation. New York: Wiley Online Library.

[26] Shi HL, Dong B, Wang WW. 2012. Features of twins and stacking faults in silver nanorice and electron-beam irradiation effect. Nanoscale 4: 6389–6392.

[27] Lábár JL, Adamik M, Barna BP, Czigány Z, Fogarassy Z, Horváth ZE, Geszti O, Misják F, Morgiel J, Radnóczi G, Székely L, Szüts T. 2012. Electron diffraction based analysis of phase fractions and texture in nanocrystalline thin films. III. Application examples. Microsc Microanal 18: 406–420.